Catalysis Today 466 (2026) 115660

Contents lists available at ScienceDirect

Catalysis Today

journal homepage: www.elsevier.com/locate/cattod

Acid gas valorization through a carbonyl sulfide (COS) intermediate over Na-containing FAU and LTA zeolites

Syeda Rabia Batool [a], Marco Fabbiani [a], Alexey Novikov [b], Raman Ghassemi [c], Soroush Zareghorbaei [c], Jeroen Lauwaert [d], Ludovic Pinard [a,*], Helene Retot [b], Joris W. Thybaut [c], Valentin Valtchev [a,*]

[a] Université de Caen Normandie, ENSICAEN, CNRS, LCS, Laboratoire Catalyse et Spectrochimie, Caen 14000, France
[b] Saint Gobain Research Provence and NORPRO, Cavaillon, France
[c] Ghent University, Laboratory for Chemical Technology, Technologiepark 125, Ghent 9052, Belgium
[d] Ghent University, Industrial Catalysis and Adsorption Technology, Valentin Vaerwyckweg, Ghent 9000, Belgium

ARTICLE INFO

Keywords:
Acid gas valorization
Carbonyl sulphide
Zeolites
Hydration level
Faujasite
Zeolite A

ABSTRACT

A promising route for the valorization of acid gas (CO_2 and H_2S) components involves their simultaneous transformation into carbon monoxide and sulfur, through carbonyl sulfide (COS) intermediate. In this work, we systematically explore the catalytic performance of 13X and 4 A for COS formation under varying conditions of temperature, acid gas partial pressure, and zeolite hydration state. H_2S, CO_2, and COS breakthrough experiments at 45 °C reveal that the capacities of all three molecules are higher for 13X than for 4 A. Thermal gravimetry on hydrated zeolites specifies water contents of 13.1 and 12.0 mmol/g for 13X and 4 A, respectively. COS yield is highest at 100 °C, showing temperature dependence in the case of 13X; in contrast, 4 A retains more than 70 % of its maximum activity over an extended range of temperatures. An increase in acid gas partial pressure from 0.2 to 0.8 bar gradually increases the total COS in 13X, whereas the activity of 4 A remains constant. Likewise, COS formation increases with decreasing zeolite hydration; threshold-dependent in 13X but progressive and relatively less pronounced in 4 A. Both zeolites, independent of conditions, undergo a decline in COS formation over time due to the water-induced inhibition of active sites, attributed to poisoning. While activity in 4 A decays rapidly, 13X exhibits a more gradual decay, corresponding to the inhibitory effect of the produced water being less pronounced in 13X than in 4 A. This reduces competitive adsorption on active sites and mitigates site blockage in 13X, which in turn preserves catalytic performance over time, indicating that 13X is more sensitive to changing conditions than 4 A. An optimum operating window identified for the two materials can help reduce the energy required for the industrial conversion of acid gas and subsequent catalyst regeneration. This corresponds to reaction at 120 °C and 250 °C and the regeneration at 250 °C and 300 °C for 13X and 4 A, respectively.

1. Introduction

A persistent environmental concern in recent years is the indiscriminate emission of anthropogenic greenhouse gases, particularly carbon dioxide (CO_2), which substantially contributes to exacerbating climate change [1]. One of the primary barriers to achieving a circular carbon economy and net-zero emissions is the lack of mature and scalable technologies for converting CO_2 into valuable chemical products. Refineries and petrochemical facilities emit approximately 1.24 Gty of CO_2 annually while also processing over 3.6 Mty of hydrogen sulfide (H_2S) [2]. The combined presence of CO_2 and H_2S in industrial streams forms what is commonly referred to as “acid gas” [3].

The simultaneous conversion of carbon dioxide (CO_2) and hydrogen sulfide (H_2S) remains a major challenge in acid gas treatment, as conventional technologies such as the Claus process, for elemental sulfur formation from H_2S, are limited in scope and do not fully exploit the chemical potential of these compounds [4–6]. In contrast, an emerging approach involves the co-conversion of CO_2 and H_2S into carbonyl sulfide (COS), followed by its thermal cracking into two valuable products [7]: elemental sulfur and carbon monoxide (CO). This pathway offers dual valorization by transforming both acid gas components into commercially relevant outputs without necessitating prior separation

* Corresponding authors.
E-mail addresses: ludovic.pinard@ensicaen.fr (L. Pinard), valentin.valtchev@ensicaen.fr (V. Valtchev).

https://doi.org/10.1016/j.cattod.2025.115660
Received 8 October 2025; Received in revised form 28 November 2025; Accepted 19 December 2025
Available online 21 December 2025

[8]. The formation of COS from CO_2 and H_2S is thermodynamically favorable under appropriate conditions [9] ([2], and its decomposition yields a clean separation of sulfur and platform molecule. This integrated transformation bypasses the limitations of current CO_2 reduction technologies, which typically require high-purity CO_2 and are incompatible with the presence of H_2S.

$$H_2S_{(g)} + CO_{2(g)} \rightleftharpoons COS_{(g)} + H_2O_{(x)}\ (x = \text{liquid/adsorbed}) \quad (1)$$

A key step in this combined approach is the formation of COS, which is thermodynamically favored when the partial pressure of water, a by-product of the reaction ([2], is minimized in the gas phase. To drive the equilibrium toward COS formation, it is crucial that (1) a catalyst is used to lower the activation barrier for COS formation by enhancing the interaction between H_2S and CO_2, and (2) the produced water remains either in the liquid phase or is effectively retained in the adsorbed phase on the catalyst or support. It has recently been shown by Pfeifer et al. that pre-loading the catalyst bed with water, before the acid gas reaction, prevents COS formation as water occupies nearly all adsorption sites, which are then blocked for CO_2 and H_2S [10]. This further signifies that the water produced during the reaction has a strong inhibiting effect by polluting the catalyst. In this context, zeolites emerge as highly effective materials, not only due to their established role in gas desulfurization but also because of their intrinsic ability to act as molecular sinks for water [4]. The strong affinity of zeolites for H_2O (with sorption capacity $H_2O \gg H_2S \geq CO_2 \approx COS$) enables them to shift the equilibrium toward COS production by selectively removing water from the reactive environment [11,12]. Furthermore, the exchangeable cations within the zeolite framework can serve as active catalytic sites, facilitating the adsorption and activation of CO_2 and H_2S [13]. These dual functionalities, water sorption and catalytic activity, render cationic zeolites well-suited for promoting COS formation under relatively mild conditions, where moderate temperature increases can further enhance the reaction yield within thermodynamic limits [9]. As water must remain adsorbed on zeolite, the reaction temperature should also be relatively low, <100 °C, to drive the equilibrium towards COS formation. However, some zeolites can also retain water efficiently at higher temperatures, thereby allowing the extension of the range of possible conditions for promoting COS formation.

Studies have focused on zeolites of the faujasite family (IZA code FAU, e.g., NaX, NaY) and Linde A (IZA code LTA, e.g., NaA), where the amount of COS formed follows the trend NaX > NaA > NaY [14]. Their structures are composed of an arrangement of cages where the Na^+ cations are distributed in positions (namely I, II, and III) at different interaction strengths with the lattice, depending on the Si/Al ratio and the presence of coordinated water with the alkali metal cations [15]. Only the larger cages (FAU super-cage or LTA cage) can be accessed by H_2S and CO_2, where weakly coordinated cations (corresponding to positions II and III for FAU and LTA zeolites) are exposed, and it is here that the reaction takes place [16]. The smaller cages (sodalite cages) can only act as water sinks [17]. The catalytic activity increases as the cation-lattice interaction decreases, and the number and type of cations influence it as well [18]. Even though there is a common agreement in the literature on the catalytic role of the cations, the precise reaction mechanism and the interplay between reagents/products and zeolite structure are often only schematically represented.

In the case of aluminum-rich FAU zeolites with Si/Al ratio up to about 2.5 (NaX-type), H_2S molecules undergo dissociative adsorption, while this is not the case for NaY-type zeolites with a Si/Al > 2.5 [19,20]. At low doses on NaX, H_2S fully dissociates, resulting in the formation of S^{2-} and 2 H^-, while at higher coverages, apart from dissociation into HS^- and H^+, physical adsorption also occurs [21]. At higher Si/Al ratios, only physisorption is most likely to happen, such as in Na-Y zeolites [22]. From the H_2S adsorption forward, little is stated on the actual mechanism of the reaction of H_2S with CO_2 [9,13,17]. Some empirical evidence and estimation of COS production are quite well established in the field. On X zeolites, it has been possible to reach 75 % H_2S conversion in batch experiments with acid gas concentration equimolar to the zeolite adsorption capacity [9]. Recently, Pfeifer et al. carried out an extensive study in dynamic conditions on LTA-type zeolites with an increasing degree of Ca exchange, emphasizing the cation position and the role of water in catalyst deactivation [13].

The efficiency of the COS formation process strongly relies on the extent of adsorption of H_2S on the active sites, as well as the retention of produced water in the adsorbed phase. As the H_2S capacity is higher at lower temperatures, the reaction is mostly carried out at temperatures lower than 100 °C. For instance, batch formation of COS on alkaline earth cation-exchanged A and X zeolites was studied at room temperature by Fellmuth et al [16]. Pfeifer et al. reported the acid gas conversion to COS at 25 °C using Ca-exchanged NaA, whereas Lutz et al. explored the room temperature activity of salt (NaBr, NaCl) modified NaX and NaY zeolites [13,17]. Similarly, Bulow et al. discussed the ambient temperature formation of COS on NaCaA zeolite under static experimental conditions of technical desulphurization of gases [9]. Interestingly, COS formation is also known to happen on non-porous amorphous silica alumina (ASA) at slightly elevated temperatures, i.e., 90 °C [23]. Therefore, the catalytic performance of COS production under a wide range of temperatures and water content in zeolites remains underexplored.

Many literature reports, exploring zeolites as adsorbents, demonstrate a substantial impact of pressure on H_2S and CO_2 uptake[24–29]. Nonetheless, most of the literature on the catalytic formation of COS has focused on specific fixed ratios of CO_2 and H_2S with a high excess of the former component. Fellmuth et al [16]. and Lutz et al [17,30]. worked with a CO_2:H_2S molar ratio of 4:1 in the feed gas, whereas Pfiefer et al [13]. studied the reaction at a 100:1 ratio. Zhang et al., while studying the COS formation over unsupported CoMo sulfide catalysts (T = 300 °C, CO_2: H_2S = 2:1), demonstrated that increasing the CO_2/H_2S molar ratio was beneficial for COS yield [4]. However, it is quite clear that a major challenge lies in the processing of the hardest acid gas compositions, i.e., H_2S:CO_2= 1:1. Cines et al. focused on the formation of COS during natural gas treatment, showing that low H_2S concentrations in the feed can play an important role in its conversion [31]. The percentage of H_2S reacted decreased with the increase in H_2S feed concentration. Chowanietz et al. explored the influence of acid gas concentration in zeolite 5 A and silica alumina gel by reducing its partial pressure through dilution with nitrogen [32]. They observed a decline in COS formation as the partial pressure of acid gas decreased. This effect is particularly pronounced with silica alumina gel, suggesting a material-dependent impact of partial pressure on catalytic COS formation. It is, therefore, essential to also inspect in detail the impact of the partial pressure of reagent gases on catalytic COS formation.

Despite the growing interest in COS-mediated acid gas valorization, a comprehensive understanding of how key operational parameters, such as reaction temperature, acid gas dilution, and the hydration state of zeolites, affect COS formation remains largely underexplored in the literature. The present work investigates the conversion of CO_2 and H_2S over two representative zeolites heavily employed in gas treatment, 13X and 4 A, by studying the role of the reaction temperature, acid gas concentration, and zeolite water retention in the catalytic COS formation. Our systematic approach lies in the exploration of reaction temperatures up to 300 °C, high concentrations of hard acid gas up to 80 % v/v, and increasingly water-saturated zeolites. The results obtained allow for evaluating the relationships between physicochemical factors governing COS formation and offer a foundation for optimizing catalyst selection, operating conditions, reaction cycling, and regeneration strategies in future acid gas upgrading technologies.

2. Materials & methods

2.1. Experimental

SiOLITE® 13X and SiOLITE® 4AH were purchased in their sodium form from Grupo IQE, hereafter 13X and 4 A, respectively. Their chemical composition was determined by inductively coupled plasma mass spectrometry (ICP-MS) on a 7900 ICP-MS from Agilent Technologies. Zeolite powders were mineralized in aqua regia (HNO_3:HCl=1:3 v/v) + HF 40 % v/v, and heated to 100 °C for 1 h, then neutralized with boric acid and the volume brought to 100 mL before analysis.

The morphology of zeolite was assessed by scanning electron microscopy (SEM) on uncoated particles with a Jeol Schottky emission scanning electron microscope JSM-IT800, operating at 3.00 kV and equipped with an upper hybrid detector (UHD) and a secondary electron detector (SED).

The textural characteristics of 13X were analyzed by nitrogen sorption at −196 °C on a Micromeritics Tristar instrument. Specific surface area (SSA) of the microporous materials is estimated according to the Brunauer-Emmet-Teller equation corrected with the Rouquerol criteria fitted within the BETSI software[33–35]. Furthermore, CO_2 physisorption isotherms for 13X and 4 A were obtained with a Micromeritics ASAP2020 instrument at 0 °C in the pressure range of 0–1.0 bar. Before N_2 and CO_2 physisorption measurements, approximately 100 mg of the sample was degassed at 350 °C under vacuum for 6 h (ramping rate: 1.5 °C/min).

The zeolites' water content was measured using thermogravimetric analysis (TGA) on a NETZSCH STA 449 instrument. Before the experiments, zeolite powder was kept in a closed chamber with NaCl-saturated solution (75 % relative humidity) for a consistent starting water content. 10 mg of such zeolite powders were weighed into an alumina crucible and heated under a 30 mL/min nitrogen flow, with a 2 °C/min ramp until reaching the target temperature, where the sample is kept for 2 h (isothermal step), then ramped to 350 °C and kept to completion of water desorption. The isothermal steps are designed to discriminate the water desorption at 45, 100, 150, 200, 250, 300 °C so that each sample is heated at one plateau to get the water loss at that specific temperature and then to 350 °C to obtain the total water loss for each run.

Cumulative breakthrough curve measurements of H_2S, CO_2, and COS, and catalytic tests on 13X and 4 A zeolites were carried out in a fixed-bed reactor from a VINCI Micro Catalytic Bed unit (Figure S1). The feed composition (H_2S:CO_2:N_2) is determined by the volume flows of each gas component using factory-calibrated mass flow controllers (MFCs) from Bronkhorst. Feed gases can be chosen from H_2S (Linde, 94.954 % v/v in N_2), CO_2 (Air Liquide, 99.995 % v/v), and COS (Air Liquide, 0.50 % v/v in N_2) bottles connected to the unit. Additionally, N_2 can be added to dilute the acid gas mixture and used as a carrier gas as well. The reactor pressure is set at 1.1 ± 0.1 bara via a dome-loaded piston backpressure regulator (BPR). Downstream of the unit, a scrubber system is used to capture and neutralize any residual sulphur-containing species.

The catalyst bed was prepared by compressing zeolite powder in a manual hydraulic press under a load of 5 tons. The resulting compacted material was subsequently ground using a mortar and pestle and sieved to obtain particles with a size distribution between 250 and 500 μm, ensuring uniformity and minimizing channeling effects during flow. The selected fraction was then loaded into a tubular reactor and subjected to thermal pretreatment under a nitrogen flow (30 mL/min) at 350 °C for 6 h (activated catalyst), unless otherwise specified for residual water studies, vide infra. The reactor geometry allows for the packing of up to 4 g of shaped material. The catalyst bed was configured with a height of 100 mm and an internal reactor diameter of 9.1 mm, resulting in a height-to-diameter ratio of approximately 10:1. This aspect ratio also maintains a particle-to-column ratio of 1:20 to minimize radial diffusion limitations and wall effects [36].

The effluent gases from the reactor unit are analyzed with an online gas chromatograph (GC) Crystal-9000 from Chromatec Analytic. The chromatograph is equipped with a 6-way sampling valve and two 60 m PLOT capillary columns: GS-GasPro (0.32 mm internal diameter) from Agilent and BP-1 (0.25 mm internal diameter) from SGE, along with a micro thermal conductivity detector (μTCD) and a flame photometric detector (FPD). The response factors of the μTCD and FPD detectors were determined through a single-point calibration at 5000 ppmv for COS and a calibration curve from 30000 up to 130000 ppmv for H_2S and CO_2. The developed GC method allows for a sampling time resolution of 5 min with a 15 min gap between each consecutive analysis run to accommodate the initial retention time.

Catalytic tests were performed in the temperature range of 45–300 °C under a continuous flow (CF) of diluted acid gas, with an H_2S:CO_2 ratio of 1:1 and concentrations ranging from 3 % to 13 % v/v each in N_2 and an acid gas weight hourly space velocity (WHSV) of 0.19 h^{-1}. A pre-saturation phase (PS) is always used to evaluate the dynamic adsorption capacities of acid gas components except for catalytic tests at different acid gas partial pressures. During this phase, a freshly activated sample was exposed to a feed composition of 13 % v/v of H_2S in N_2, with a total feed WHSV of 0.53 h^{-1}. Then, the feed composition was adjusted to achieve the desired concentration, typically 13 % v/v for each acid gas component, while maintaining a constant total flow rate (Figure S2). Catalytic tests were also done, varying the acid gas partial pressure at constant temperature. For this, the reaction was performed at 100 °C with the total feed WHSV ranging between 0.74 and 0.90 h^{-1}, by diluting with nitrogen while keeping the constant H_2S:CO_2 molar ratio (1:1). The feed acid gas to nitrogen ratios varied as follows; 1:4, 2:3, 3:2, 4:1 v/v (acid gas WHSV of 0.19, 0.38, 0.57 and 0.77 h^{-1}, respectively). The conversion of acid gas components, COS yield, and total COS produced are calculated as follows:

$$X_j(\%) = \frac{y_j^{in} - y_j^{out}}{y_j^{in}} \times 100 \quad (2)$$

$$Y_j(\%) = \frac{y_{COS}^{out}}{y_j^{out}} \times 100 \quad (3)$$

$$Q_{COS} = \frac{\dot{n}_j^{in}}{100 \times m_{cat}} \int_{t_0}^{t_1} \frac{y_{COS}^{out}}{y_j^{out}} dt \quad (4)$$

Where X_j is conversion, Y_j is yield, and Q_{COS} is the total COS formed per gram of zeolite (mmol/g). y is the molar percentage drawn from chromatographic peak area and detector response factor, and j is the acid gas component index.

$\dot{n}_j^{in}$: inlet flow rate of acid gas component (mmol/min)

m_{cat}: mass of catalyst (g)

3. Results and discussion

3.1. Physicochemical characterisation

: Zeolites 13X and 4 A consist of alternating tetrahedra of SiO_4 and AlO_4^- as primary building units with general formulas $Na_{88}[Si_{104}Al_{88}O_{384}]$-FAU and $Na_{96}[Si_{96}Al_{96}O_{384}]$-LTA, respectively. The spare negative charge carried by the presence of aluminium in the structure is compensated by cations, Na in the case of the considered zeolites. The three-dimensional arrangement of the tetrahedra forms the sodalite cages (*sod*) that are connected either by six-membered rings prism (D6R) or four-membered rings prism (D4R), forming the frameworks of FAU and LTA, respectively [37]. These two zeolite structures are different in the effective pore diameters and the distribution of Na cations. The frameworks are characterized by a central cavity of 11.4 Å in diameter that is accessible through 12-membered ring openings with apertures of ~7.4 Å for FAU, while smaller 8-membered ring windows with apertures of ~4.1 Å are typical for LTA, as shown in Fig. 1(top). The

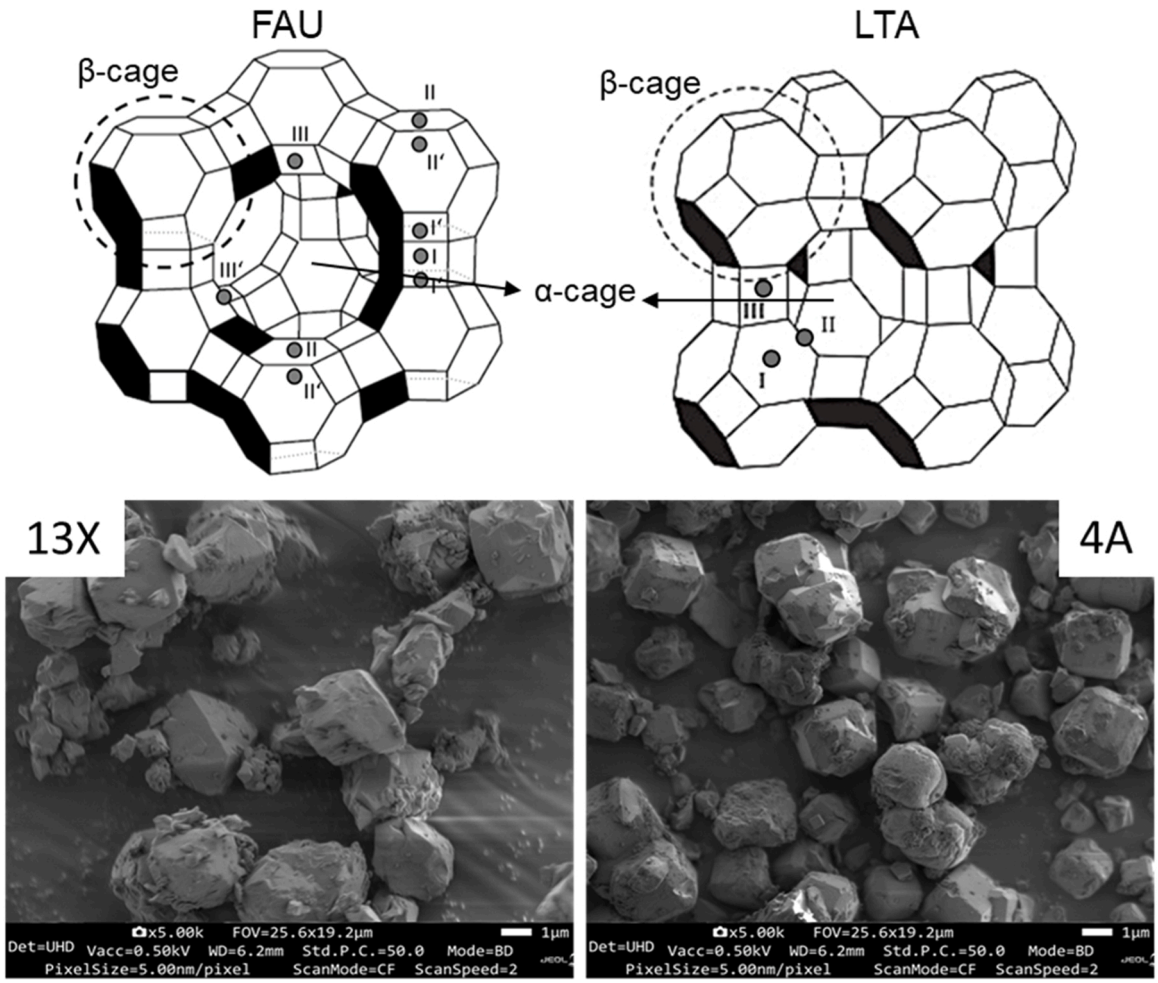

Fig. 1. Framework structures of FAU and LTA framework showing α- and β-cages and cationic positions (top), adopted from [39,40] and SEM micrographs of 13X and 4 A samples used in this work (bottom).

SEM micrographs of the two materials are presented in Fig. 1(bottom). 13X crystals exhibit octahedral morphology, whereas those of 4 A show cubic morphology with cut-off edges and corners, and the crystal size of the two zeolites ranges from 2 to 4 μm [37,38].

Table 1 presents the physicochemical properties of the two zeolites, showing that 13X has a slightly higher Si/Al molar ratio and Na content compared to 4 A. The X-ray diffraction patterns and adsorption isotherms of the two materials are presented in Figure S3. As is well known in the literature, the microporosity of 4 A cannot be probed with N_2 adsorption at −196 °C. Indeed, effects such as cation gating, diffusion restrictions, and weak N_2-cation interaction lead to an important underestimation of the specific surface area of Na-LTA samples, which can be accessed either by the means of ion exchange or by using CO_2 at 0 °C [41] as is the case here (Figure S4). The results on CO_2 adsorption show that 13X zeolite exhibits a higher Langmuir surface area than 4 A zeolite, where a higher uptake is attributed to the larger and more accessible pore structure of the FAU structure, which is in line with previous studies [13,41,42].

a. calculated from ICP-MS), b. from N_2 isotherms at −196 °C (Figure S4, left), c. from CO_2 isotherms at 0 °C (Figure S4, right).

Table 1
Chemical and textural properties of zeolites 13X and 4 A.

Label	Si/Al[a] (mol/mol)	Na/Al[a] (mol/mol)	BET SSA[b] N_2 (m^2/g)	Langmuir SSA[c] CO_2 (m^2/g)
13X	1.2	0.94	890	770
4 A	0.97	0.88	15	596

3.2. Zeolite water content

To evaluate the effect of water presence on the catalytic COS formation, the residual water content of zeolites treated at different temperatures (45, 100, 150, 200, 250, 300, 350 °C, hereafter named isothermal steps) is systematically measured using TGA, starting from hydrated zeolites. In Fig. 2, the relative mass of the samples (top) and the residual water content (bottom) are presented for the two zeolites treated at different isothermal steps. The maximum water capacity, independently of the isothermal step used, is 23.6 % and 21.0 % of the 13X and 4 A sample total mass, corresponding to 13.1 and 12.0 mmol of water per gram, respectively. These values are comparable with water uptake at 25 °C reported in the literature for similar materials [25,43]. The results from the isothermal steps curves show that for temperatures higher than 100 °C, 13X retains, on average, less water than 4 A. This difference is most pronounced after 250 °C, where residual water is equivalent to 2.2 % (0.3 mmol/g) and 8.3 % (1.0 mmol) of the total water for 13X and 4 A, respectively. Most of the loosely bound water (below 150 °C) is released to a similar extent in both zeolites, whereas the amount of strongly bound water differs significantly between the two zeolites. In the case of 13X, the larger pores and a less restrictive framework allow easier desorption of water at elevated temperatures, whereas 4 A retains water more resiliently due to the small pore size and stronger confinement effects [39,40].

Based on the analysis of TGA curves as shown in Fig. 2, zeolite hydration levels are calculated as follows and plotted as a function of temperature (Fig. 2).

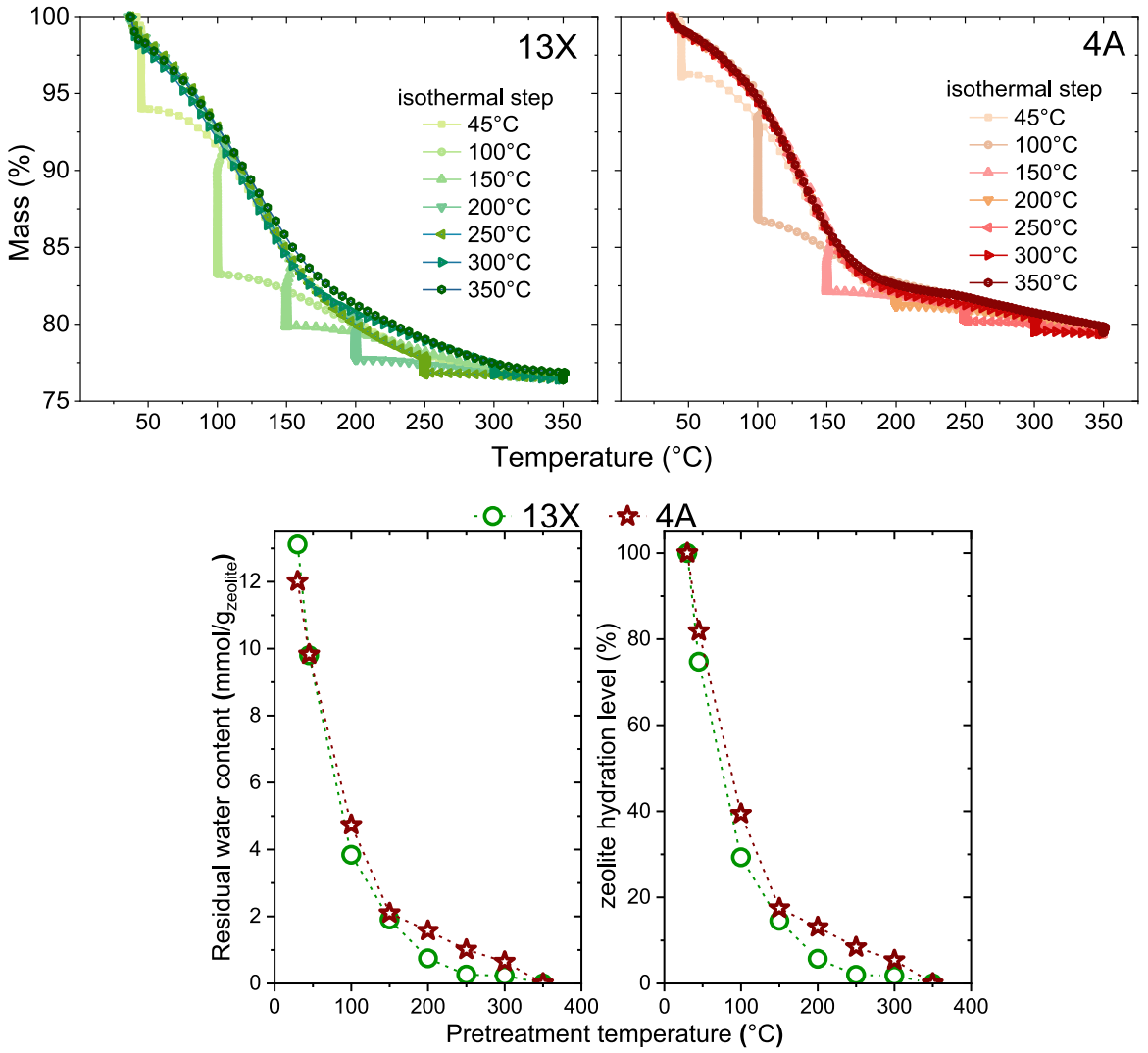

Fig. 2. TGA curves with isothermal steps for 13X (top left) and 4 A (top right). Water content (bottom left) and zeolite hydration level (bottom right) as a function of isothermal step. Total water lost during each isothermal step and the respective residual water contents in mmoles of H_2O per gram and per unit cell of zeolite are presented is Table SI.

$$Zeolite\ Hydration\ level(\%) = 100 - \frac{water\ loss\ at\ isothermal\ step}{total\ water\ loss\ at 350\ ^{\circ}C} \times 100 \quad (5)$$

For example, the total water lost by 13X during the whole TGA run from 30 to 350 °C amounts to 23.6 % whereas that lost during the isothermal step of 100 °C amounts to 16.7 %. Based on the above equation, the corresponding zeolite hydration level is calculated to be 29.3 %. To study the effect of residual water on the COS formation at 100 °C (vide infra), hydration levels for isothermal steps ≥ 100 °C are considered.

3.3. Dynamic adsorption capacities

A baseline estimation of the catalysts' dynamic sorption capacities at 45 °C is done with breakthrough experiments for H_2S, CO_2, and COS on 13X and 4 A, (Figure S5 (top)), and is presented in Fig. 3. The adsorption capacities of all three molecules for 13X are higher compared to 4 A. This is the consequence not only of the difference in the number of accessible cations, but also their positioning and accessibility play an important role in the molecules' adsorption [25,44].

The difference in dynamic capacities for 13X and 4 A is most significant (~80 %) in the case of COS (0.5 mmol/g for 13X and 0.1 mmol/

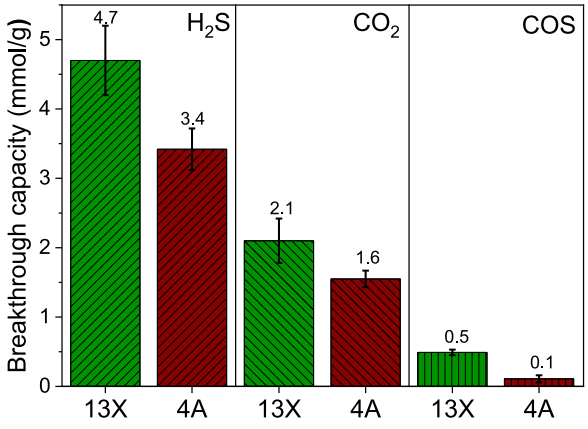

Fig. 3. Breakthrough capacities of H_2S (//), CO_2 (\\) and COS (||) for 13X and 4 A calculated from breakthrough curves at 45 °C and 1.1 bar (bottom). Feed: 13 % v/v of H_2S or CO_2 in N_2, 0.5 % v/v of COS in N_2. All the dynamic adsorption capacities were measured using identically activated samples (activation at 350 °C for 6 h).

g for 4 A, respectively). Whereas this difference amounts to ~28 % for H_2S (4.7 mmol/g for 13X and 3.4 mmol/g for 4 A, respectively) and ~24 % for CO_2 (2.1 mmol/g for 13X and 1.6 mmol/g for 4 A, respectively). Thus, the capacities of the four adsorptive molecules, irrespective of zeolitic material, follow the same order: $H_2O > H_2S > CO_2 >$COS, which is consistent with previous results on excess isotherms of 13X [25]. For 4 A, however, excess isotherms in the literature under similar conditions indicate a lower CO_2 uptake than COS [44], which can likely be due to the differences between equilibrium vs. dynamic measurements.

Our results nevertheless suggest that under dynamic conditions, COS exhibits stronger effective affinity than CO_2 on 13X and 4 A. The relatively higher uptake of COS compared to CO_2 likely arises from its greater polarizability and stronger interaction with cationic sites, making CO_2 adsorption the limiting factor for sustaining the reaction [22]. Starke et al. showed that the number of available cations responsible for dissociative adsorption (chemisorption) is three times higher in the case of 13X than in 4 A [39,40]. This is because the structure of the two zeolites leads to different cation distribution, which consequently influences the number of cations available for chemisorption [40]. At a Si/Al ratio of 1.2, the unit cell of FAU (13X) contains 88 Na^+ cations, position I and II occupy 32 cations each, whereas the remaining 24 cations are occupied by site III. Thus, there are 56 accessible sites; the supercage-accessible Na^+ located at site II (on the 6-ring facing the supercage) and site III (near the 12-ring window), which are less coordinated and more directly involved in adsorbate interactions [40]. By contrast, LTA (4 A), at a Si/Al ratio of 1, contains 96 Na^+ cations per unit cell, distributed as 8 cations at site I in the sodalite cages, 3 at site II (at the 8-ring window), and 1 at site III (in the 4-membered ring), which is sterically more constrained. Here, 32 Na^+ cations at sites II and III of the supercage are considered accessible [39]. Table 2 lists the adsorption capacities of H_2S, CO_2, COS, and H_2O normalized to the Na^+ content in the supercages. For 13X, this ratio is 1.63, 0.55, 0.62, and 4.47 for H_2S, CO_2, COS, and H_2O, respectively. In contrast, the corresponding values for 4 A are 2.14, 0.75, 0.92, and 7.50, reflecting the smaller number of accessible cations per unit mass of zeolite. Thus, although the dynamic capacities are higher for 13X, the effective loading per accessible cation is higher in LTA. This indicates that, in 4 A, each supercage cation accommodates a larger fraction of the adsorbed molecules, which may intensify site blocking effects and contribute to a faster inhibition of the acid gas conversion with respect to 13X. The fact that chemisorption holds a large contribution towards total capacity, as proposed by Starke et al [40], is in favour of 13X exhibiting H_2S capacity higher than 4 A, which is also true in our case.

3.4.Effect of reaction temperature: To elucidate the distinct catalytic behaviours of these materials, particular attention is given to their performance at 100 °C, which is the temperature at which the highest total COS yield is observed (vide infra). Fig. 4 displays the COS yield as a function of time-on-stream over 13X and 4 A zeolites at 100 °C, whereas COS yields and CO_2 conversions across a range of reaction temperatures (45–300 °C) are presented in Figures S7 and S8. For 13X, the COS yield initially increases with time, reaching a maximum before undergoing a gradual decay. This latter trend is indicative of a progressive reaction inhibition, primarily attributed to the accumulation of co-produced water on the active sites of the zeolite [13,17], given the significantly higher affinity of water to Na cations compared to H_2S, CO_2, and COS [11,12]. 13X still retains some water adsorption capacity at 100 °C (3.8 mmol/g), enabling partial uptake of the generated water. Competitive adsorption among CO_2, H_2S, and COS is inherent to the system; as the reaction proceeds, the build-up of water further intensifies the phenomenon by introducing another competing adsorbate. This competitive adsorption mechanism aligns with observations by Pfeifer et al., who reported analogous behavior for COS formation over 4 A zeolite at ambient temperature, where water leaves the reactor as the last component of the feed mixture when the reactivity is then extinguished [13]. Additionally, the build-up of water induces a roll-up effect (Figure S11), which is symptomatic of adsorbing water displacing previously retained reactants, thus further altering the adsorption equilibrium and contributing to the loss of catalytic activity over time.

Zeolite 4 A exhibits a high COS peak yield, approximately 2.5 times greater than that observed for 13X under identical conditions. However, this elevated performance is short-lived as COS yield rapidly drops below 8 % within the first 60 min of reaction, while 13X keeps about 24 %. The apparent COS yield over 4 A exceeds 100 % due to strong adsorption of H_2S, CO_2, and by-product water, which delays the breakthrough of reactants while COS desorbs rapidly. As shown by the instantaneous yield definition in [4], the total amount of COS coming out is higher than the total amount of CO_2 that enters the reactor. As a result of this temporary suppression of CO_2 flow at the reactor outlet, caused by strong CO_2 uptake, combined with rapid COS release from the bed, drives apparent yields above 100 % even though the time-integrated yield remains $\leq$ 100 %. This transient imbalance reflects kinetic and adsorption dynamics rather than a true stoichiometric excess.

The difference in catalytic behavior of the two zeolites highlights the influence of the zeolite framework on COS formation kinetics and the catalyst's ability to remain active towards acid gas conversion. The slower decrease in the COS yield observed for 13X may be attributed to its larger number of accessible active sites compared to 4 A [40]. Consequently, while water produced during the reaction progressively adsorbs onto these sites, only a portion of them is inhibited at a given time, allowing residual activity to persist over extended durations. This suggests that the total water uptake during the reaction remains below the maximum adsorption capacity of 13X, thereby avoiding complete site saturation. However, since the reaction is confined to the α-cage while the measured water capacity (from TGA) involves both α- and β-cages, the effective tolerance toward water (1.42 mmol/g, calculated from evolved COS at 100 °C) is in fact lower than that indicated by total water uptake (3.8 mmol/g, calculated from TGA isothermal step at 100 °C), and only the α-cage-associated capacity is directly exploitable for sustaining COS formation. In contrast, 4 A not only offers fewer active sites but also suffers from significant steric hindrance due to its smaller pore openings and stronger confinement of molecules within the α-cages. The diffusion limitations inherent to the 8-MR structure of 4 A likely intensify the progressive inhibition, as restricted pore access impedes the transport of both, reactants and products. This likely restricts molecular access and diffusion, accelerating the inhibition of active sites by water and leading to rapid poisoning with limited to no reusability of active sites under these conditions. Thus, on 4 A, the produced water acts as a strong poison: once the produced water (1.29 mmol/g at 100 °C) occupies all the available sites in the α-cages, conversion becomes nearly null, although the zeolite's total water capacity (4.7 mmol/g, calculated from the TGA isothermal step at 100 °C) is not reached.

Given the distinct COS yield profiles exhibited by the two zeolites and the multiple factors that we consider, i.e., temperature-dependent water mobility/capacity/adsorption strength in the zeolite, it is crucial to examine the cumulative COS formation as a function of reaction temperature across different time intervals to understand the trends of COS evolution. Fig. 5 presents the quantity of COS produced during three specific periods: 0–60 min, 60–180 min, and the total amount formed over 180 min of reaction. While both 13X and 4 A exhibit temperature-dependent behavior, it manifests differently between the

Table 2
Ratio of adsorption capacity of H_2S, CO_2, and COS (mmol/g) at 45 °C and 1.1 bar with respect to Na content (mmol/g) available in the supercages. The values in the parentheses give the ratio of adsorption capacity with respect to the total Na content of zeolite (mmol/g).

Label	H_2S/Na	CO_2/Na	COS/Na	H_2O/Na
13X	1.63 (1.03)	0.55 (0.35)	0.62 (0.40)	4.47 (2.88)
4 A	2.14 (0.71)	0.75 (0.25)	0.92 (0.30)	7.50 (2.50)

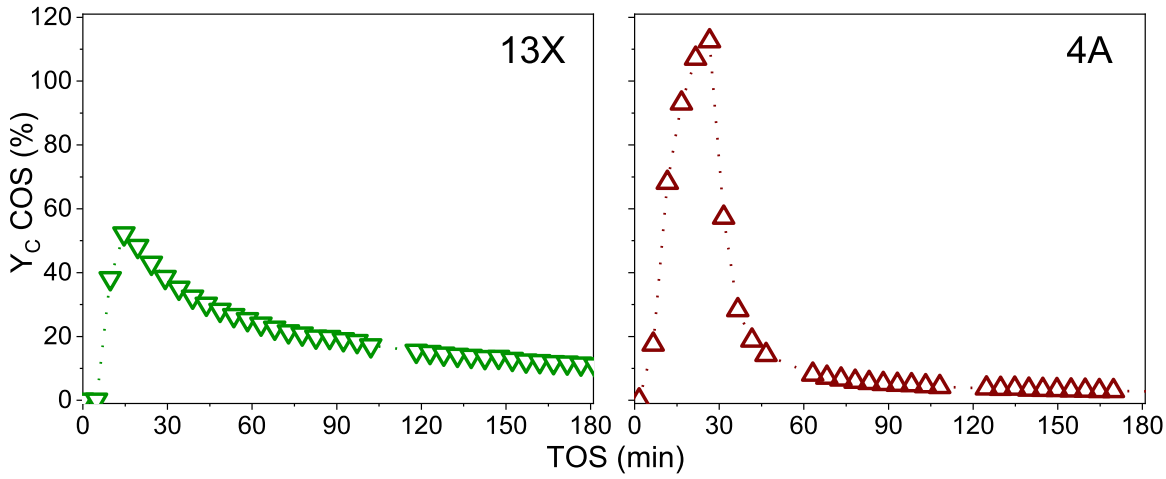

Fig. 4. COS yield as a function of temperature over 13X (left) and 4 A (right). Reaction temperature 100 °C, 0.27 bar acid gas partial pressure, 0.17 h^{-1} acid gas WHSV, and 0 % initial hydration level.

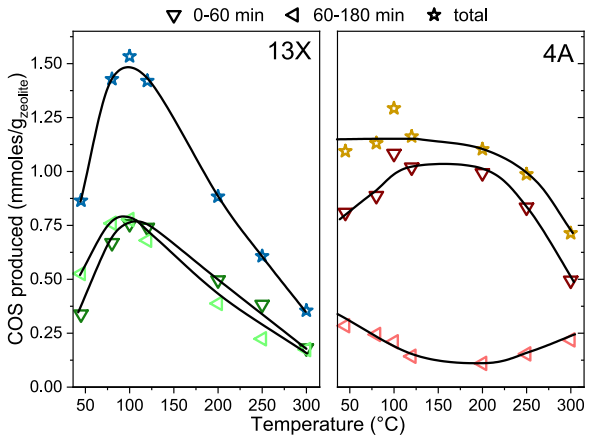

Fig. 5. Cumulative COS produced as a function of temperature over 13X (left) and 4 A (right). 0.27 bar acid gas partial pressure, 0.17 h^{-1} acid gas WHSV, and 0 % initial hydration level. The solid black lines are drawn as a guide for the eye.

two materials. Despite the lower H_2S capacity of both materials at 100 °C compared to 45 °C (Figure S6), COS production is higher in both zeolites at 100 °C, possibly due to enhanced kinetics and improved diffusion.

COS formation on zeolite 13X exhibits a pronounced temperature dependence, reaching a maximum at 100 °C before decreasing at higher temperatures. In contrast, zeolite 4 A shows minimal dependence on temperature, with total COS production remaining relatively constant across the tested temperature range, in line with the findings of Bulow et al [9]. in the lower temperature range and Fellmuth et al [16]. at wider ranges. In particular, the quasi-plateau extending up to 250 °C indicates a steady activity regardless of temperature variation. Interestingly, it produces similar amounts of COS at 45 °C and 200 °C, despite being at fairly different levels of water capacity at these temperatures, which further suggests that the COS formation in 4 A is not as strongly governed by the extent of water adsorption as in the case of 13X.

Moreover, while on 4 A more than 90 % of the COS is produced during the first hour, zeolite 13X continues to generate significant quantities of COS beyond the first hour, maintaining a production rate comparable to that observed during the initial 60 min. Overall, these observations reflect two distinct mechanistic behaviours governed by the interaction of water with the zeolite framework. Zeolite 4 A, limited by steric and diffusional constraints, is strongly inhibited by the produced water, and once active sites in α-cages are completely saturated by produced water, the reaction is essentially precluded under thermodynamic equilibrium conditions, leading to negligible conversion. By contrast, zeolite 13X shows a more progressive inhibition effect of water, which is evident in its temperature-dependent performance and sustained COS productivity.

As previously discussed, the efficiency of COS formation depends not only on the adsorption capacity of H_2S but also on the effective retention of reaction-generated water within the zeolite pores. One of the primary motivations for studying this reaction at low temperatures, as emphasized in earlier literature [16,40,45], is the well-documented decrease in H_2S adsorption capacity at higher temperatures (Figures S5 and S6). However, a potentially underexplored factor is the existence of an optimal temperature window, higher than what is typically used for acid gas conversion [9,13,16,17], in which the amount of chemisorbed H_2S remains sufficiently high. At the same time, the co-produced water is still retained within the porous structure, clearly not up to the zeolite's maximum water capacity, as capacity decreases with temperature. This condition is critical for maintaining the availability of active sites and, therefore, the overall catalytic activity retention of the produced water in the adsorbed phase on the catalyst drives the equilibrium towards COS formation. Our detailed temperature-dependent study demonstrates that efficient COS formation is achievable even at elevated temperatures, although the optimal operating window is clearly material-dependent. For zeolite 13X, maximum activity is observed within the range of 80–120 °C, whereas 4 A can retain significant performance until 250 °C.

When extending catalytic tests to higher temperatures, questions naturally arise regarding the thermal stability and reusability of zeolite catalysts. Repeated exposure to elevated temperatures and successive activity-regeneration cycles could potentially compromise the structural integrity of the materials. X-ray diffraction (XRD) patterns of spent materials compared to freshly prepared samples (Figure S3) revealed no significant changes in relative crystallinity or phase composition. These findings confirm the thermal robustness of the zeolites under reaction and regeneration conditions, indicating that both 13X and 4 A zeolites retain their structural integrity.

3.5. *Effect of acid gas partial pressure*

To evaluate the effect of acid gas dilution on COS formation, catalytic experiments were performed varying the partial pressures of H_2S:CO_2 mixture, while maintaining their stoichiometric 1:1 molar ratio. These tests were conducted at 100 °C, as optimal conditions for COS formation based on prior screening results (Figure S9). Fig. 6 presents the

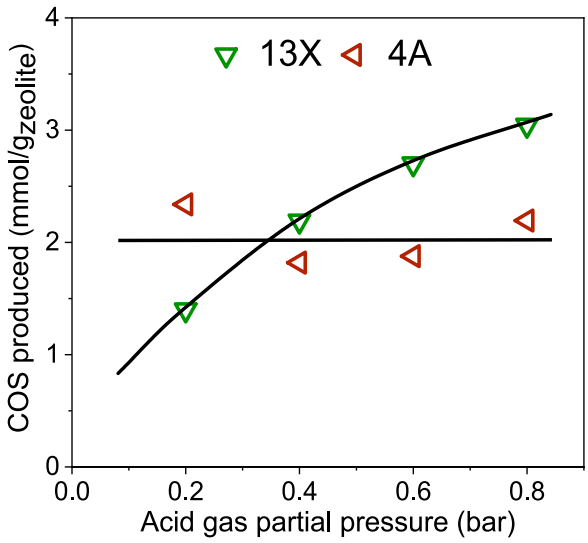

Fig. 6. Cumulative COS produced during 180 min of reaction as a function of acid gas partial pressure for 13X and 4 A. Reaction temperature 100 °C, acid gas WHSV of 0.19–0.77 h^{-1}, 0 % initial hydration level. The solid black lines are drawn as a guide for the eye.

cumulative COS produced as a function of acid gas partial pressure for zeolites 13X and 4 A.

On one hand, 13X shows a direct correlation of the COS produced with the increase of the acid gas partial pressure. This dependency does not seem to be perfectly linear, as at high concentrations it deviates towards lower amounts of COS. On the other hand, 4 A shows a rather flat behavior, settling around 2 mmol/g of COS produced throughout the whole range of considered pressures. Interestingly, the two curves intersect at ~0.4 bar, where both zeolites produce similar amounts of COS. Below and above this threshold, dilution effects become important: 13X continues to benefit from increasing acid gas partial pressure, while 4 A remains largely insensitive. These observations illustrate that the COS formed on 13X increases with partial pressure due to the kinetic effect, i.e., higher reactant concentration leads to faster COS formation within the same reaction time. In contrast, the flat response of 4 A suggests early site saturation, which prevents further increases in COS formation despite higher feed pressure.

If we compare the 100 °C condition from Fig. 5 to the first acid gas partial pressure point from Fig. 6, both of these are conducted at the same temperature and acid gas WHSV. However, between these two cases, the total feed WHSV increased from 0.57 to 0.74h^{-1} , i.e., the acid gas to carrier gas ratio decreased from 0.36 to 0.25. Under these changes, COS production in 13X decreased from 1.53 to 1.39 mmol/g, consistent with lower reactant concentration. In contrast, COS production on 4 A increases from 1.29 to 2.33 mmol/g under the same conditions. In agreement with the previously discussed rapid poisoning in 4 A, this result also suggests that higher dilution of the feed limits water build-up on active sites, which delays inhibition and allows more COS to form, not due to improved intrinsic reactivity but by kinetically mitigating poisoning effects.

3.6. *Effect of zeolite hydration level*

Since water strongly inhibits reactivity by strongly adsorbing on active sites, it is important to determine the threshold at which the effect becomes sufficiently pronounced to hinder the material's catalytic performance. To analyse the COS production at different hydration levels, the catalyst is pre-treated at various temperatures ranging from 100 to 350 °C. Afterward, pre-saturation in H_2S at 100 °C is carried out, followed by the reaction at 100 °C. The maximum zeolite hydration level refers to the one calculated from the isothermal step at 100 °C (29 % and 39 % in 13X and 4 A, respectively). It is important to note that the dehydration of a fully hydrated zeolite removes water not only from the supercages but also from the sodalite cages. When considering the acid gas conversion, the sodalite cages can merely act as water reservoirs, and the Na^+ cations at site I in the sodalite cages do not contribute to the catalytic activity. Fig. 7 shows the total COS produced at 100 °C during two reaction intervals as a function of zeolite hydration level, whereas COS yields as a function of zeolite hydration levels are presented in Figure S10.

The total COS generally decreases exponentially with an increase in the water content of both zeolites, with an exponential decay constant of −0.26 and −0.1 for 13X and 4 A, respectively (Fig. 7 and Figure S12). The exponential decay constants, obtained from fitting COS produced vs. hydration level, are not kinetic rate constants but rather empirical descriptors of water sensitivity: they quantify the relative steepness of COS decay with increasing hydration. A more negative exponential constant for 13X indicates a faster suppression of COS formation relative to 4 A as the hydration level increases. In 13X, the most significant increase in total COS occurs in the final dehydration step, from 5.7 % to 2 %. Subsequent drying results in only slight improvements in activity. This proposes that most of the active sites remain inaccessible for COS formation until 5.7 %, despite an observed increase in COS yield as compared to that of fully hydrated zeolite. Once a critical threshold is crossed, i.e., 5.7–2 %, water is removed from the sites relevant for acid gas conversion, such as Na^+ cations positioned at II and III sites in the super cages, enabling a sharp increase in activity. Since most of the active sites are already free, further dehydration resulted in only a slight increase in activity. In contrast, a progressive recovery of activity of 4 A from hydrated to a fully dry zeolite is observed, which suggests that even small amounts of water significantly affect access to active sites. Owing to the narrow pores and lower total site accessibility (as compared to 13X), each water molecule (adsorbed or desorbed) has a stronger impact on catalytic function. As explained earlier, 4 A produces more than 90 % of the total COS during the first hour, whereas 13X yields comparable amounts during the 0–60 min and 60–180 min intervals. Following this, it can be observed that as the zeolite water content of 13X increases, COS formation decreases exponentially, with a slope of −0.25 and −0.26 during 0–60 min and 60–180 min, respectively. In contrast, in the case of 4 A, COS production as a function of hydration level decreases with slopes of −0.13 and −0.08 during the 0–60 min and 60–180 min periods, respectively. Thus, independent of the reaction interval, the hydration level sensitivity of 13X for COS formation is more pronounced

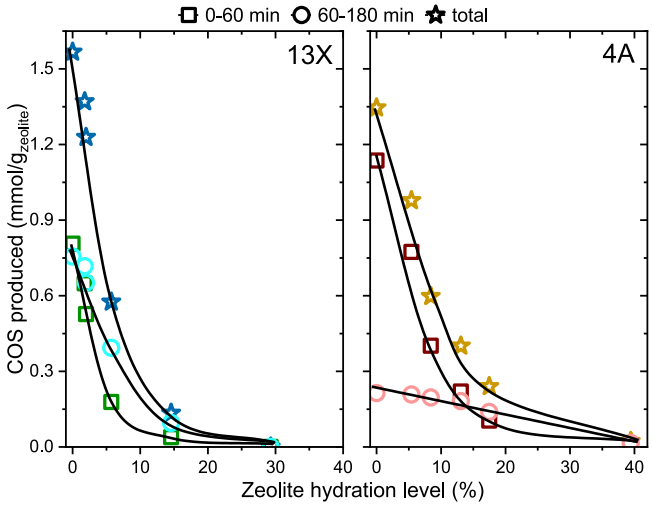

Fig. 7. Cumulative COS produced as a function of zeolite hydration levels for 13X and 4 A. Reaction temperature 100 °C, 0.27 bar acid gas partial pressure, 0.17 h^{-1} acid gas WHSV, and 0 % initial hydration level. The solid black lines are drawn as a guide for the eye.

than 4 A.

In summary, in 13X, the impact of hydration on COS formation is non-linear, threshold-dependent, and even the low hydration levels block the key adsorption/reaction sites. On the other hand, the smaller, more confined and uniformly hydrated structure of 4 A delays the blocking of active sites, allowing it to sustain catalytic activity across a broader spectrum of hydration levels and giving a hydration-dependent recovery of activity. These results demonstrate that the nuances in pore size, cage geometry, and the arrangement and accessibility of cations between 13X and 4 A play a crucial role in determining how zeolite hydration level influences COS formation.

While it is evident that COS yields decrease in both materials with the increase in hydration level, it is important to highlight the optimal hydration regime, where zeolite still retains more than 70 % of its activity. This regime ranges up to 2 % hydration in 13X and 5.4 % in 4 A, corresponding to activation of the zeolite at 250 °C and 300 °C, respectively. The investigation of optimal reaction temperature and hydration conditions in this study is highly relevant for the industrial valorization of acid gas, as operating at elevated reaction temperatures and enabling catalyst regeneration under conditions proximate to the reaction temperatures can substantially reduce energy requirements and enhance overall process efficiency.

4. Conclusions

This work compares the performance of zeolites 13X and 4 A for converting CO_2 and H_2S into COS and establishes how their structural properties govern activity under different operating conditions. Zeolite 13X shows higher adsorption capacities for H_2S, CO_2, and COS than 4 A, owing to its higher number of low-coordinated Na^+ cations as well as more favorable pore geometry for molecular uptake. For both materials, H_2S is the most strongly adsorbed species, followed by CO_2 and COS, respectively. Catalytic tests carried out across wide ranges of temperature, pressure, and zeolite hydration levels reveal that the two materials behave very differently as conditions change. COS formation over 13X increases with both temperature (up to 100 °C) and acid-gas partial pressure, whereas 4 A displays 4 A exhibits a quasi-plateau over the studied temperature and pressure ranges. Both zeolites reach their highest COS yields at 100 °C. The impact of zeolite hydration level is threshold-dependent in 13X but is progressive and relatively less pronounced in 4 A. The strong inhibitory effect of water, in 4 A, limits reactivity essentially to the initial cation-site interactions, leading to a faster decrease in activity. In contrast, the comparatively weaker inhibition in 13X allows additional catalytic activity to be sustained, resulting in gradual activity decay. Overall, 13X is more sensitive to changes in temperature, pressure, and hydration, while 4 A is dominated by strong water inhibition and rapid loss of activity. Identification of optimal balance between reaction temperature and zeolite hydration, detailed in this work, will help reduce energy demand and improve the efficiency of industrial acid gas valorization by enabling catalyst regeneration near reaction temperatures. In addition, this work also provides a foundation for modelling existing gas-treatment processes and enhancing the treatment of similar gaseous streams.

CRediT authorship contribution statement

Marco Fabbiani: Writing – original draft, Validation, Methodology, Formal analysis, Conceptualization. **Joris W. Thybaut:** Writing – review & editing, Validation, Funding acquisition. **Valentin Valtchev:** Writing – review & editing, Validation, Supervision, Funding acquisition. **Syeda Rabia Batool:** Writing – original draft, Investigation, Formal analysis, Conceptualization. **Soroush Zareghorbaei:** Writing – review & editing. **Jeroen Lauwaert:** Writing – review & editing. **Ludovic Pinard:** Writing – review & editing, Writing – original draft, Validation, Supervision, Methodology. **Helene Retot:** Writing – review & editing. **Alexey Novikov:** Writing – review & editing. **Raman Ghassemi:** Writing – review & editing.

Declaration of Competing Interest

The authors declare that they have no known competing financial interests or personal relationships that could have appeared to influence the work reported in this paper.

Acknowledgments

This work has been supported by the e-CODUCT project, funded under Horizon Europe Grant Agreement n°101058100.

Appendix A. Supporting information

Supplementary data associated with this article can be found in the online version at doi:10.1016/j.cattod.2025.115660

Data availability

No data was used for the research described in the article.

References

[1] V. Masson-Delmotte, P. Zhai, A. Pirani, S.L. Connors, C. Péan, S. Berger, N. Caud, Y. Chen, L Goldfarb, M.I. Gomis, M. Huang, K. Leitzell, E. Lonnoy, J.B.R. Matthews, T.K. Maycock, T. Waterfield, Ö. Yelekçi, R. Yu, B. Zhou, Climate Change 2021: The Physical Science Basis. Contribution of Working Group I to the Sixth Assessment Report of the Intergovernmental Panel on Climate Change, Cambridge University Press: Cambridge, United Kingdom and New York, NY, USA, 2021, 10.1017/9781009157896.

[2] EU ETS. https://climate.ec.europa.eu/eu-action/eu-emissions-trading-system-eu-ets_en.

[3] E. Grynia, J.J. Carroll, P.J. Griffin, Advances in gas processing, in: F. Benyahia, F. T. Eljack (Eds.), Dehydration of Acid Gas Prior to Injection. Proceedings of the 2nd Annual Gas Processing Symposium, 2010, pp. 177–185, https://doi.org/10.1016/S1876-0147(10)02020-3.

[4] F. Zhang, Z. Wei, G. Jiang, G. Li, M. Zhao, Z. Zhang, J. Cheng, Z. Hao, Synergistic conversion of acid gases (H2S and CO2) to valuable chemicals: carbonyl sulfide synthesis over vacancy-defective CoMo sulfide catalysts, Appl. Catal. B Environ. 319 (2022) 121912–121922, https://doi.org/10.1016/j.apcatb.2022.121912.

[5] J. Eow, Recovery of sulfur from sour acid gas: a review of the technology, Environ. Prog. 21 (2002) 143–162, https://doi.org/10.1002/ep.670210312.

[6] M. Sassi, A.K. Gupta, Sulfur recovery from acid gas using the claus process and high temperature air combustion (HiTAC) technology, Am. J. Environ. Sci. 4 (5) (2008) 502–511.

[7] e-CODUCT – Greenhouse gas and acid gases conversion by electrothermal catalysis. https://e-coduct.eu/ (accessed 2025-09-26)..

[8] Q. Zhou, P. Wu, C. Liu, J. He, W. Jiang, Highly selective conversion of H2S/CO2 and reaction mechanism with CeO2 loading of MgO as catalysts, Ind. Eng. Chem. Res. 62 (17) (2023) 6660–6671, https://doi.org/10.1021/acs.iecr.3c00257.

[9] M. Bülow, W. Lutz, M. Suckow,, The mutual transformation of hydrogen sulphide and carbonyl sulphide and its role for gas desulphurization processes with zeolitic molecular sieve sorbents, Stud. Surf. Sci. Catal. 120 (1999) 301–345, https://doi.org/10.1016/S0167-2991(99)80556-4.

[10] Pfeifer, S.; Pasel, C.; Bläker, C.; Eckardt, T.; Klinkenberg, N.; Eggebrecht, J.; Gleichmann, K.; Bathen, D. Mechanistic Investigation of Catalytic Cos Formation on Ion-Exchanged Lta Zeolites During Fixed-Bed Adsorption. 2025, 113729–113738 https://doi.org/10.2139/ssrn.5167316..

[11] M. Abdirakhimov, M.H. Al-Rashed, J. Wójcik, Recent attempts on the removal of H2S from various gas mixtures using zeolites and waste-based adsorbents, Energies 15 (15) (2022) 5391–5410, https://doi.org/10.3390/en15155391.

[12] X. Chen, B. Shen, H. Sun, G. Zhan, Ion-exchange modified zeolites X for selective adsorption desulfurization from claus tail gas: experimental and computational investigations, Microporous Mesoporous Mater. 261 (2018) 227–236, https://doi.org/10.1016/j.micromeso.2017.11.014.

[13] S. Pfeifer, C. Pasel, C. Bläker, T. Eckardt, N. Klinkenberg, J. Eggebrecht, K. Gleichmann, D. Bathen, catalytic COS formation on ion-exchanged LTA zeolites during adsorption, Microporous Mesoporous Mater. 383 (2025) 113408, https://doi.org/10.1016/j.micromeso.2024.113408.

[14] M.R. Cines, D.M. Haskell, C.G. Houser, Molecular sieves for removing H2S from natural gas, Chem. Eng. Prog. 72 (8) (1976).

[15] T. Frising, P. Leflaive, Extraframework cation distributions in X and Y faujasite zeolites: a review, Microporous Mesoporous Mater. 114 (1–3) (2008) 27–63, https://doi.org/10.1016/j.micromeso.2007.12.024.

[16] P. Fellmuth, W. Lutz, M. Billow, Influence of weakly coordinated cations and basic sites upon the reaction of HzS and C02 on zeolites, Zeolites 7 (4) (1987) 367–371.

[17] W. Lutz, A. Seidel, B. Boddenberg, On the formation of COS from H_2S and CO_2 in the presence of zeolite/salt compounds, Adsorpt. Sci. Technol. 16 (7) (1998) 577–581, https://doi.org/10.1177/026361749801600707.
[18] E.O. Fetisov, M.S. Shah, C. Knight, M. Tsapatsis, J.I. Siepmann, Understanding the reactive adsorption of H_2S and CO_2 in sodium-exchanged zeolites, ChemPhysChem 19 (4) (2018) 512–518, https://doi.org/10.1002/cphc.201700993.
[19] H.G. Karge, J. Raskó, Hydrogen Sulfide Adsorption on faujasite-type zeolites with systematically varied Si-AI ratios, J. Colloid Interface Sci. 64 (3) (1978) 522–532.
[20] H. Lechert, H.J. Hennig, Das Verhalten Der Protonen- Und Der 23Na-Resonanz in Zeolithen Vom Faujasittyp in Abhängigkeit von Der Belegung Mit Schwefelwasserstoff 76 (5_6) (1971) 319–327, https://doi.org/10.1524/zpch.1971.76.5_6.319.
[21] H.G. Karge, M. Ziółek, M. Łaniecki, U.v./Vis and i.r. Spectroscopic Study of Hydrogen Sulphide Adsorption on Faujasite-Type Zeolites, Zeolites 7 (3) (1987) 197–202, https://doi.org/10.1016/0144-2449(87)90050-9.
[22] M. Gaillard, V. Montouillout, F. Maugé, C. Fernandez, An Infrared and Solid-State NMR Study of the H2S Adsorption on Basic Zeolite, Stud. Surf. Sci. Catal. 154 (2004) 1679–1685, https://doi.org/10.1016/S0167-2991(04)80694-3.
[23] Mesters. A Process for the Manufacture of Sulphide Compounds. WO2011084973A1, July 14, 2011..
[24] L.H.de Oliveira, J.G. Meneguin, M.V. Pereira, E.A.da Silva, W.M. Grava, J.F. do Nascimento, P.A. Arroyo, H2S Adsorption on NaY Zeolite, Microporous Mesoporous Mater. 284 (2019) 247–257, https://doi.org/10.1016/j.micromeso.2019.04.014.
[25] K.G. Wynnyk, B. Hojjati, R.A. Marriott, High-Pressure Sour Gas and Water Adsorption on Zeolite 13X, Ind. Eng. Chem. Res. 57 (2018) 15357–15365, https://doi.org/10.1021/acs.iecr.8b03317.
[26] F. Bandarchian, M. Anbia, Conventional Hydrothermal Synthesis of Nanoporous Molecular Sieve 13X for Selective Adsorption of Trace Amount of Hydrogen Sulfide from Mixture with Propane, J. Nat. Gas. Sci. Eng. 26 (2015) 1380–1387, https://doi.org/10.1016/j.jngse.2015.08.019.
[27] E. Pérez-Botella, M. Palomino, G.B. Báfero, H.O. Pastore, S. Valencia, F. Rey, The Influence of Zeolite Pore Topology on the Separation of Carbon Dioxide from Methane, J. CO2 Util. 72 (2023) 102590–102593, https://doi.org/10.1016/j.jcou.2023.102490.
[28] H. Maghsoudi, M. Soltanieh, Simultaneous Separation of H2S and CO2 from CH4 by a High Silica CHA-Type Zeolite Membrane, J. Membr. Sci. 470 (2014) 159–165, https://doi.org/10.1016/j.memsci.2014.07.025.
[29] Y. Zhang, Y. Guo, S. He, H. Guo, L. Luo, M. Li, T. Zhu, T. Guo, Y. Deng, Regulation of Water and Sulfur Resistance and Study of Carbon Dioxide Adsorption Properties on FAU Zeolites, Chem. Eng. J. 513 (2025) 162720–162728, https://doi.org/10.1016/j.cej.2025.162720.
[30] W. Lutz, M. Suckow, M. Bülow, Adsorption of Hydrogen Sulphide on Molecular Sieves, Gas. Sep. Purif. 4 (4) (1990) 190–196, https://doi.org/10.1016/0950-4214(90)80041-i.
[31] Cines, MR and Haskell, DM and Houser, CG. Sulfur Compound Cleanup: Molecular Sieves for Removing H/Sub 2/S from Natural Gas. Chem. Eng. Prog. (United States). 1976, 72(8).
[32] V. Chowanietz, C. Pasel, T. Eckardt, A. Siegel, D. Bathen, Formation of Carbonyl Sulfide (COS) on Different Adsorbents in Natural Gas Treatment Plants, Oil Gas. Eur. Mag. 42 (2) (2016) 82–85.
[(33)] J.W. Osterrieth, J. Rampersad, D. Madden, N. Rampal, L. Skoric, B. Connolly, M. D. Allendorf, V. Stavila, J.L. Snider, R. Ameloot, How Reproducible Are Surface Areas Calculated from the BET Equation? Adv. Mater. 34 (27) (2022) 2201502–2201513.
[34] A. Galarneau, D. Mehlhorn, F. Guenneau, B. Coasne, F. Villemot, D. Minoux, C. Aquino, J.-P. Dath, Specific Surface Area Determination for Microporous/Mesoporous Materials: The Case of Mesoporous FAU-Y Zeolites, Langmuir 34 (47) (2018) 14134–14142, https://doi.org/10.1021/acs.langmuir.8b02144.
[35] H. Azzan, D. Danaci, C. Petit, R. Pini, Unary Adsorption Equilibria of Hydrogen, Nitrogen, and Carbon Dioxide on Y-Type Zeolites at Temperatures from 298 to 393 K and at Pressures up to 3 MPa, J. Chem. Eng. Data 68 (12) (2023) 3512–3524, https://doi.org/10.1021/acs.jced.3c00504.
[36] C. Shen, M. Li, J. Ji, X. Yang, L. Li, Y. Wu, Effect of Packing Structure Evolution on the Flow Characteristics in a Binary Composite Packed Bed Based on DEM-CFD Method, Processes 11 (3) (2023) 732–750, https://doi.org/10.3390/pr11030732.
[37] R. Xu, W. Pang, J. Yu, Q. Huo, J. Chen. Chemistry of Zeolites and Related Porous Materials: Synthesis and Structure, John Wiley & Sons, 2009.
[38] S. Bahraminia, M. Anbia, E. Koohsaryan, Hydrogen Sulfide Removal from Biogas Using Ion-Exchanged Nanostructured NaA Zeolite for Fueling Solid Oxide Fuel Cells, Int. J. Hydrog. Energy 45 (55) (2020) 31027–31040, https://doi.org/10.1016/j.ijhydene.2020.08.091.
[39] A. Starke, C. Pasel, C. Bläker, T. Eckardt, J. Zimmermann, D. Bathen, D.C. S. Azevedo, Impact of Na+ and Ca2+ /on the adsorption of H2S on binder-free LTA zeolites, Adsorpt. Sci. Technol. (2021) 5531974–5531985, https://doi.org/10.1155/2021/5531974.
[40] A. Starke, C. Pasel, C. Bläker, T. Eckardt, J. Zimmermann, D. Bathen, Investigation of the adsorption of hydrogen sulfide on Faujasite zeolites focusing on the influence of cations, ACS Omega 7 (48) (2022) 43665–43677, https://doi.org/10.1021/acsomega.2c04606.
[41] E. Khoramzadeh, M. Mofarahi, C.-H. Lee, Equilibrium adsorption Study of CO2 and N2 on synthesized zeolites 13X, 4A, 5A, and beta, J. Chem. Eng. Data 64 (12) (2019) 5648–5664, https://doi.org/10.1021/acs.jced.9b00690.
[42] C.A. Grande, R. Blom, Cryogenic adsorption of methane and carbon dioxide on zeolites 4A and 13X, Energy Fuels 28 (10) (2014) 6688–6693.
[43] J.H. Jacobs, C.E. Deering, K.L. Lesage, M.J. Stashick, R.A. Marriott, Rapid Cycling Thermal Swing Adsorption Apparatus: Commissioning and Data Analyses for Water Adsorption of Zeolites 4A and 13X Over 2000 Cycles, Ind. Eng. Chem. Res. 60 (19) (2021) 7487–7494, https://doi.org/10.1021/acs.iecr.1c00469.
[44] K.G. Wynnyk, B. Hojjati, P. Pirzadeh, R.A. Marriott, High-pressure sour gas adsorption on zeolite 4A, Adsorption 23 (1) (2017) 149–162, https://doi.org/10.1007/s10450-016-9841-6.
[45] M. Bülow, Comments on the publication “use of zeolites for the removal of H2S: a mini-review” by mehtap ozekmekci, gozde salkic and mehmet ferdi fellah, fuel processing technology, 139, 49–60, November 2015, Fuel Process. Technol. 142 (2016) 396, https://doi.org/10.1016/j.fuproc.2015.10.031.